

Showcasing research from Larysa Baraban laboratory,  
Department of Radioimmunology, Helmholtz Center  
Dresden Rossendorf, Dresden, Germany.

Coexistence of fluorescent *Escherichia coli* strains in  
millifluidic droplet reactors

In order to understand the complex microbial communities,  
it is indispensable to discover the most critical factors  
influencing coexistence between species. We use a  
millifluidic system to study the multi-species bacterial  
growth to unveil the details of cooperation between two  
*Escherichia coli* strains inside droplet reactors. This system  
also has the potential for studies of multidrug resistant  
strains and drug resistance transfer.

As featured in:



See Gianarelio Cuniberti,  
Larysa Baraban *et al.*,  
*Lab Chip*, 2021, 21, 1492.


 Cite this: *Lab Chip*, 2021, 21, 1492

## Coexistence of fluorescent *Escherichia coli* strains in millifluidic droplet reactors†

 Xinne Zhao,<sup>ab</sup> Rico Illing,<sup>ac</sup> Philip Ruelens,<sup>d</sup> Michael Bachmann,<sup>b</sup> Gianarelio Cuniberti,<sup>id</sup>\*<sup>a</sup> J. Arjan G. M. de Visser<sup>d</sup> and Larysa Baraban<sup>id</sup>\*<sup>ab</sup>

Understanding competition and cooperation within microbiota is of high fundamental and clinical importance, helping to comprehend species' evolution and biodiversity. We co-encapsulated and cultured two isogenic *Escherichia coli* strains expressing blue (BFP) and yellow (YFP) fluorescent proteins into numerous emulsion droplets and quantified their growth by employing fluorescence measurements. To characterize and compare the bacterial growth kinetics and behavior in mono and co-culture, we compared the experimental observations with predictions from a simple growth model. Varying the initial ratio ( $R_0$ ) of both cell types injected, we observed a broad landscape from competition to cooperation between both strains in their confined microenvironments depending on start frequency: from a nearly symmetric situation at  $R_0 = 1$ , up to the domination of one subpopulation when  $R_0 \gg 1$  (or  $R_0 \ll 1$ ). Due to competition between the strains, their doubling times and final biomass ratios ( $R_1$ ) continuously deviate from the monoculture behavior. The correlation map of the two strains' doubling times reveals that the  $R_0$  is one of the critical parameters affecting the competitive interaction between isogenic bacterial strains. Thanks to this strategy, different species of bacteria can be monitored simultaneously in real-time. Further advantages include high statistical output, unaffected bacteria growth, and long-time measurements in a well-mixed environment. We expect that the millifluidic droplet-based reactor can be utilized for practical clinical applications, such as bacterial antibiotic resistance and enzyme reaction kinetics studies.

 Received 30th November 2020,  
 Accepted 16th March 2021

DOI: 10.1039/d0lc01204a

[rsc.li/loc](http://rsc.li/loc)

### Introduction

Understanding the functions and dynamics of microbial communities, their competition or cooperation, is fundamental for humankind.<sup>1–4</sup> The whole human microbiome contains about 100 trillion cells, 99% of which are bacteria.<sup>5,6</sup> For instance, there are as many as 400 species of beneficial, harmful, and neutral bacteria that coexist in the human gut; their balance directly affects the health of the host.<sup>7</sup> The fight over limited factors needed for microbial life such as space and food leads to natural selection.<sup>8,9</sup> Still, it is shown that the competition does not lead to a loss of

biodiversity, as co-benefits through cooperation also promote long-term coexistence.<sup>10</sup>

To better understand complex microbial communities, it is indispensable to discover the most critical factors influencing coexistence between species. In particular, it is crucial to address the aspect of what factors determine microbial coexistence.<sup>11,12</sup> In order to address the question, it is essential to set up a model to simulate the natural environment and to be able to: monitor each member of the community over a long time, precisely tune and control the microenvironment, and infer informative parameters (such as growth rate, duration of the lag phase, and final population) for analysis.<sup>13</sup>

Cellular and microbial co-culture systems have been put forward for a long time.<sup>14–16</sup> Typically, bacterial coexistence is studied in solid or well-mixed liquid environments.<sup>17</sup> In solid cultures, bacteria occupy and grow in different areas, which helps isolate and count colonies of co-cultured strains, but direct interaction between bacteria is limited.<sup>18–21</sup> Liquid system may better reflect aspects of the natural environment in which bacteria coexist in the body, such as the digestive system.<sup>22,23</sup>

However, co-culturing microbiota in a liquid environment poses challenges to differentiating and monitoring the kinetics of two or more strains simultaneously and high

<sup>a</sup> Institute for Materials Science, Max Bergmann Center of Biomaterials, Technische Universität Dresden, 01062 Dresden, Germany.

E-mail: [gianaurelio.cuniberti@tu-dresden.de](mailto:gianaurelio.cuniberti@tu-dresden.de)

<sup>b</sup> Helmholtz-Zentrum Dresden Rossendorf, Institute of Radiopharmaceutical Cancer Research, Bautzner Landstraße 400, 01328 Dresden, Germany.

E-mail: [l.baraban@hzdr.de](mailto:l.baraban@hzdr.de)

<sup>c</sup> Helmholtz-Zentrum Dresden Rossendorf, Institute of Ion Beam Physics and Materials Research, Bautzner Landstraße 400, 01328 Dresden, Germany

<sup>d</sup> Department of Genetics, Wageningen University, Arboretumlaan 4, 6703 BD Wageningen, The Netherlands

† Electronic supplementary information (ESI) available. See DOI: 10.1039/d0lc01204a

throughput quantitative analysis.<sup>24</sup> An effective differentiation method is to genetically modify bacterial strains with an inherited fluorescent reporter, which efficiently monitors the kinetics of different strains co-cultured in a liquid environment by fluorescence microscopy or flow cytometry.<sup>25–27</sup> For example, Guo<sup>28</sup> and Terekhov<sup>29</sup> successfully monitored the cell number of two co-culture bacterial strains with fluorescent microscopy by detecting unique fluorescent proteins expressed within each strain. However, data collection and analysis require a considerable amount of work. Besides, the low resolution of frequency data introduces analysis errors. In comparison, a microfluidic approach would be more effective in tracking the bacterial interaction in near real-time. It can simulate a more realistic environment in practical applications, such as predicting the response of bacteria to antibiotics; however, so far is mostly used for single strain monitoring.<sup>30–32</sup>

We used the millifluidic droplets reactor system to monitor two *Escherichia coli* strains' coexistence, reading their fluorescences in two parallel detector channels. We co-cultured these two strains in various inoculum ratios  $R_0$  (ranging from  $10^{-3}$  up to  $10^3$ ). Because of the subtle intrinsic differences in growth kinetics between the two strains (*E. coli* YFP grows faster than *E. coli* BFP), even without a specific design of the selective environment (*e.g.*, the addition of antibiotics, restriction of nutrients, or alteration of carbon sources), simply adjusting  $R_0$  can influence competition and advantage between the different strains as well. The co-culture results were described in terms of the comparison of the biomass ratio  $R_1$  at the end of the exponential phase ( $T = 10$  hours), the doubling time ( $\tau_B$ : doubling time of *E. coli* BFP;  $\tau_Y$ : doubling time of *E. coli* YFP), and the competition coefficients ( $C_{by}$  and  $C_{yb}$ ,  $C_{by}$  is the effect of *E. coli* YFP on *E. coli* BFP and  $C_{yb}$  is the effect of *E. coli* BFP on *E. coli* YFP). Besides, based on the experimentally obtained monoculture growth curves, we used a modeling approach based on Baranyi–Roberts model<sup>33</sup> and two-strain Lotka–Volterra competition model<sup>34</sup> to predict microbial growth in a mixed culture and compare it with co-culture experimental results.<sup>35</sup> The change in biomass ratio at the end of the exponential phase showed that the greater the difference between the initial cell density of two strains (when  $R_0 \gg 1$  or  $R_0^{-1} \gg 1$ ), the greater the ratio fold change ( $\log_{10}(R_1/R_0)$ ). In other words, the negative frequency-dependence at the level of yield occurred between two strains.<sup>36</sup> The competition coefficient calculated from the ratio of the Malthusian parameters<sup>37</sup> between co-culture and monoculture also shows that it is affected by the initial frequency of the two strains. Specifically, similar to the competition coefficient, we found a positive frequency-dependence of growth rates of the two strains (*i.e.*, faster doubling times for larger initial frequencies). Our results show that the millidroplet approach comprehensively tracks the growth dynamic of two co-cultured strains in real-time. We expected this strategy to guide future applications in multi-strain co-culture monitoring and drug resistance studies.

## Results and discussion

### Millifluidic droplet detectors dual-channel for coexistence studies

We designed the millifluidic setup for automatic droplets readout to perform large-scale high-resolution competition assays and calibration measurements of each strain separately. Fig. 1a–g depicts a schematic diagram of the millifluidic system, divided into two main areas: for droplet generation and for detection.

In the droplet formation module, syringes and pumps (Nemesys pump, Cetonic) are used to co-inject the microbes and oily phases into cross-junction. Therefore, the aqueous droplets are generated by shear force. The hydrofluoroether oil (HFE) with 1% PicoSurf surfactant serves as a continuous phase to maintain the water in oil emulsion stable. The droplet sequence (contains up to 500 droplets) is transferred to a storage coil, then to the detection area.

In the detection area, we designed a double fluorescent detector element to measure the abundance of two *E. coli* strains (*E. coli* BFP: MG1655 galK::mTagBFP2-FRT and *E. coli* YFP: MG1655 galK::SYFP2-FRT). Since the fluorescence proteins expressed by two strains have distinct fluorescence excitation and emission spectra (see Fig. S1† for details), we specifically selected light sources and filters for two detection modules (BFP detection light source  $\lambda_1 = 385$  nm, filter  $\lambda_{Ex} = 390/18$  nm,  $\lambda_{Em} = 460/60$  nm; YFP detection light source  $\lambda_1 = 505$  nm, filter  $\lambda_{Ex} = 497/16$  nm,  $\lambda_{Em} = 535/22$ , Thorlabs). A fluidic pump (Harvard, PHD-2200) controls the droplet sequence flow forward and backward through the detectors by infusing and refilling the circuit with the HFE oil. The whole system is interfaced with LabView software, which automatically measures the growth curves of two strains with high precision during hours (see details in ES1†).<sup>31,32</sup>

### Cell density in droplets analyzer

First, we calibrated the relationship between fluorescent signal and cell density for each strain (Fig. S2†). We determined the limits of detection (LODs) of the droplets analyzer of *E. coli* BFP around 5650 cells per droplet, and the LODs of *E. coli* YFP is 6000 cells per droplet. We also checked the two strains' mixed-signal and compared them with the single strain signal (in Fig. S3†). The cross-tested results eliminate the possibility of signal interference and prove that the fluorescent signal can genuinely reflect the bacteria's growth status.

### YFP and BFP monocultures analysis

Growth kinetics of bacteria can be accurately described by the bacterial growth curve, according to the growth model of J. Monod.<sup>27,38,39</sup> Here, the reference growth curves of monoculture with various initial cell densities were first measured (Fig. 1h and i, the initial cell density means the initial inoculum cell concentration in each droplet). Both bacterial strains were also analyzed as monoculture using the

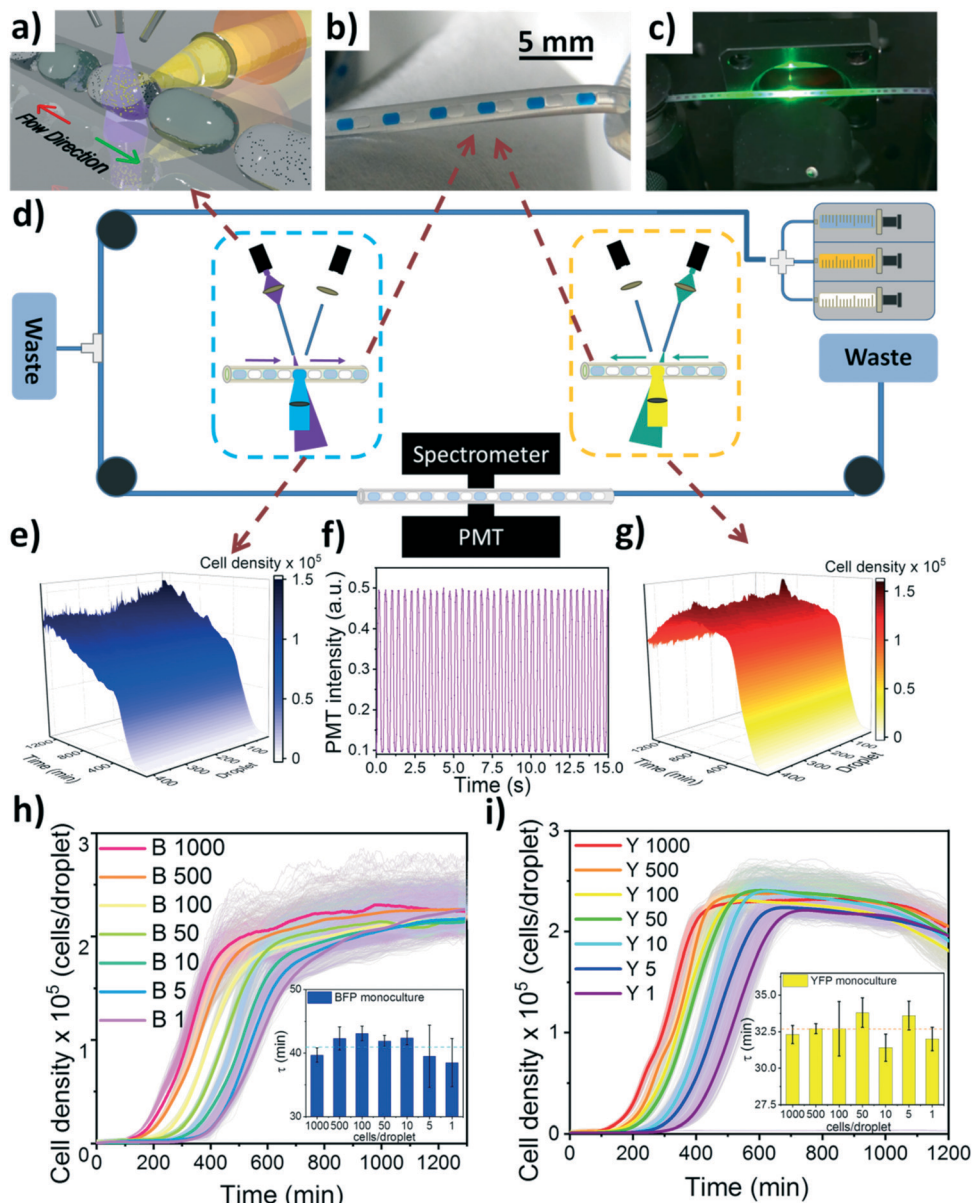


**Fig. 1** Sketch of setup. a) The monitoring of *E. coli* BFP cultured in the droplet by UV light; b) a combination with water droplets (blue) and clear mineral oil droplet in the tubing; c) the optical fiber from the LED focus on the droplet; d) sketch of setup with two detection modes; e) 3D growth curves of *E. coli* BFP detected under UV light when droplet sequence moving forward and g) *E. coli* YFP detected under cyan LED light while droplet sequence moving backward; f) the fluorescent signal caught up by PMT when droplet contains bacteria passing by the detector. The comparison of *E. coli* BFP and *E. coli* YFP monoculture growth curves as well as doubling time. h) The family and average growth curves of *E. coli* BFP monoculture and their doubling time (insert) with an initial cell density of 1000, 500, 100, 50, 10, 5, 1 cells per droplet. i) The family and average growth curves of *E. coli* YFP monoculture and their doubling time (insert) with an initial cell density of 1000, 500, 100, 50, 10, 5, 1 cells per droplet. Error bars show the standard error of the mean.

batch culture method in shaking flasks. Their cell number was measured over time in a photometer (optical density at a wavelength of 600 nm,  $OD_{600}$ ), as shown in Fig. S4†

Both methods demonstrate that the final population yield is slightly different for both strains (higher for YFP signal). Besides, the doubling time of two strains also has slight differences (YFP grow faster). Simultaneously, we did not observe significant differences between the doubling time of monoculture induced by the different initial cell

densities. However, the detection of lag-phase-time shifted due to the LODs.

Notably, the fluorescent methods of analysis (e.g., microscopy, fluorescent plate reader, and flow cytometry) show that the *E. coli* YFP monoculture growth curves exhibit an evident decline of fluorescence signal after 1000 min. However, *E. coli* BFP shows a continued slow increase in the growth curves during the stationary phase. We further obtained the growth curves with different methods (Fig. S5a–

d†), in various media (Fig. S5e and f†), as well measured the cell size, pH value, and the cell alive rate change (see details in ESI†, Fig. S5 and S6). By comparing the results obtained between different methods, we suggest these differences observed in the late stationary phases of YFP and BFP are associated with the various fluorophore stability and photobleaching rates. For instance, YFP fluorescent signal decrease is related to the degradation of the fluorescent protein, which is affected by the pH value, fluorescent lifetime, and cell state, but not cell size.<sup>40–43</sup> The comparison of light intensity and exposure time in different detection devices is shown in Table S4 in ESI†.

To avoid the influences of the photobleaching effects on competition studies, in the following, we analyze the growth curves of both strains until the time frame when the stationary phase starts. Namely, we took the ratio  $R_1$  from the start point of the stationary phase (after culturing 10 hours).

### Predict co-culture by modeling

The monoculture model (Baranyi–Roberts model<sup>33</sup>) was first fitted to monoculture growth experimental data, then the co-culture model (2-strain Lotka–Volterra competition models<sup>34</sup>) to co-culture experimental competition data. The relative co-culture growth of both strains is predicted by using the estimated growth and competition parameters with the Python code programmed by Y. Ram *et al.*<sup>35</sup> From the modeling prediction results, we found the biomass ratios (at the beginning of the stationary phase) have the same trend as the results obtained from the droplet reactor, which is the lower the relative initial frequency, the higher its comparable yield. It indicates that the millifluidic droplet strategy has an excellent ability to track bacterial strains and reflect their growth in co-culture separately.

### Bacteria co-culture with different $R_0$

Compared to monocultures, we found (i) negative frequency-dependent interactions for final biomass and (ii) positive frequency-dependent effects on growth rate in the co-cultures.

To determine the competitive relationship between two bacterial strains, we encapsulated them into the droplets with a specific  $R_0$  (the ratio between initial cell density of *E. coli* BFP  $B_0$  and *E. coli* YFP  $Y_0$ ). Then we took the  $R_0$  as a variable from  $10^{-3}$  to  $10^3$  for each parallel experiment and collected the growth data by droplet-based millifluidic automatic setup<sup>31,32</sup> (the ‘ratio’ represents the proportion of *E. coli* BFP to *E. coli* YFP, and the ‘fraction’ is used to describe the proportion of *E. coli* BFP or *E. coli* YFP to the total co-culture cell density). Ratio  $R_0 = 1$  is reached by injecting 1000 cells of each strain into droplets (1000:1000). Other values of  $R_0$  are achieved by the serial decrease of the cell numbers of the other strain, down to the extreme value 1000:1 (and 1:1000) for BFP/YFP, respectively.

Subsequently, we comprehensively characterized the bacterial competition dynamics by comparing the average doubling time and their variance, maximum cell concentration,

$R_1$ , ratio fold change, and competition coefficients. Furthermore, by comparing different methods such as flow cytometry, photometer, plate reader, and co-culture curves modeling and prediction, our system is shown to precisely and efficiently track bacteria competitive dynamics.

By contrasting the growth curves of two strains and their combination under various  $R_0$ , two strains' behavior changes can be intuitively observed. When  $R_0 = 1$ , the *E. coli* YFP appeared earlier and grew faster than *E. coli* BFP, as shown in Fig. 2a. This advantage is also observed in monoculture by millidroplet reactor, plate reader, and photometer (Fig. 2, S4 and S5†). However, when  $R_0 = B_0/Y_0 > 2$ , this advantage gradually disappeared with the further increase of  $R_0$  (Fig. 2(b–g) for  $R_0 > 1$ , and Fig. 2(h–m) for the  $R_0 < 1$ ). From the final combination of the growth curves, we observed all groups with different  $R_0$  reached a similar maximum cell density  $C_{max}$  of around  $2.5 \times 10^5$  cells per droplet, indicating that  $R_0$  does not affect total final biomass.

Notably, even in extreme ratios such as  $R_0 = 10^3$  (Fig. 2g) or  $R_0 = 10^{-3}$  (Fig. 2m), the bacterial strain with lower initial frequency can still survive. The comparison of  $R_1$  with  $R_0$  tells us how the composition changes under different  $R_0$  (Fig. 3a). The larger  $R_0$  leads to larger  $R_1$ , but we clearly state  $R_1 = R_0$  is the “null expectation” when competitive interactions between both strains do not affect fitness, *i.e.*, ratio of Malthusian parameters = 1. When  $R_0$  is scaled from  $10^3$  to  $10^{-3}$  ( $\log_{10} R_0$  is from 3 to -3),  $R_1$  constantly reduces and shows a trend to narrow the gap of population size between the two strains, indicating a negative frequency-dependent effect on yield for both strains. When  $R_0 = 1$  ( $\log_{10} R_0 = 0$ ),  $R_1 = 0.579$ , suggesting that *E. coli* YFP is more fit than *E. coli* BFP in a co-culture environment. From  $R_0 = 1$  to  $10^3$  or  $10^{-3}$ , the initial fraction between *E. coli* BFP and *E. coli* YFP become more and more unmatched; a clear asymmetry between the  $R_1$  shows up and constantly amplifies. This phenomenon is more clearly described in Fig. S7 (ESI†). From  $R_0 = 1$  to  $10^3$  or  $10^{-3}$ , the ratio fold change reverses from negative to positive, but its absolute value increases all along. In other words, the lower the relative initial frequency, the higher its relative yield. To sum up, the competition hierarchy inversion occurred between two strains and constantly approached the stable coexistence. We confirmed that this phenomenon is caused by  $R_0$ , and not by the experimental method, by counting cell numbers with different devices such as fluorescent microscopy, flow cytometry, and plate reader (see details in Fig. S8–S10, Tables S1 and S2†). We also predicted the co-culture growth curves and compared them with experimental growth curves (see details in Fig. S11†).<sup>35</sup> For most of the prediction curves, the  $C_{max}$  (the final cell density at  $T = 10$  hours) reaches a similar level as the experimental results. All the estimated growth curves of *E. coli* BFP match relatively well with the experiment result. The *E. coli* YFP has a longer lag time ( $R_0 \leq 1$ ) and less  $C_{max}$  ( $R_0$  from 100 to 10) in prediction results.

Moreover, the  $R_1$  detected and calculated in different ways were compared in Fig. S12 (ESI†). All results point to the

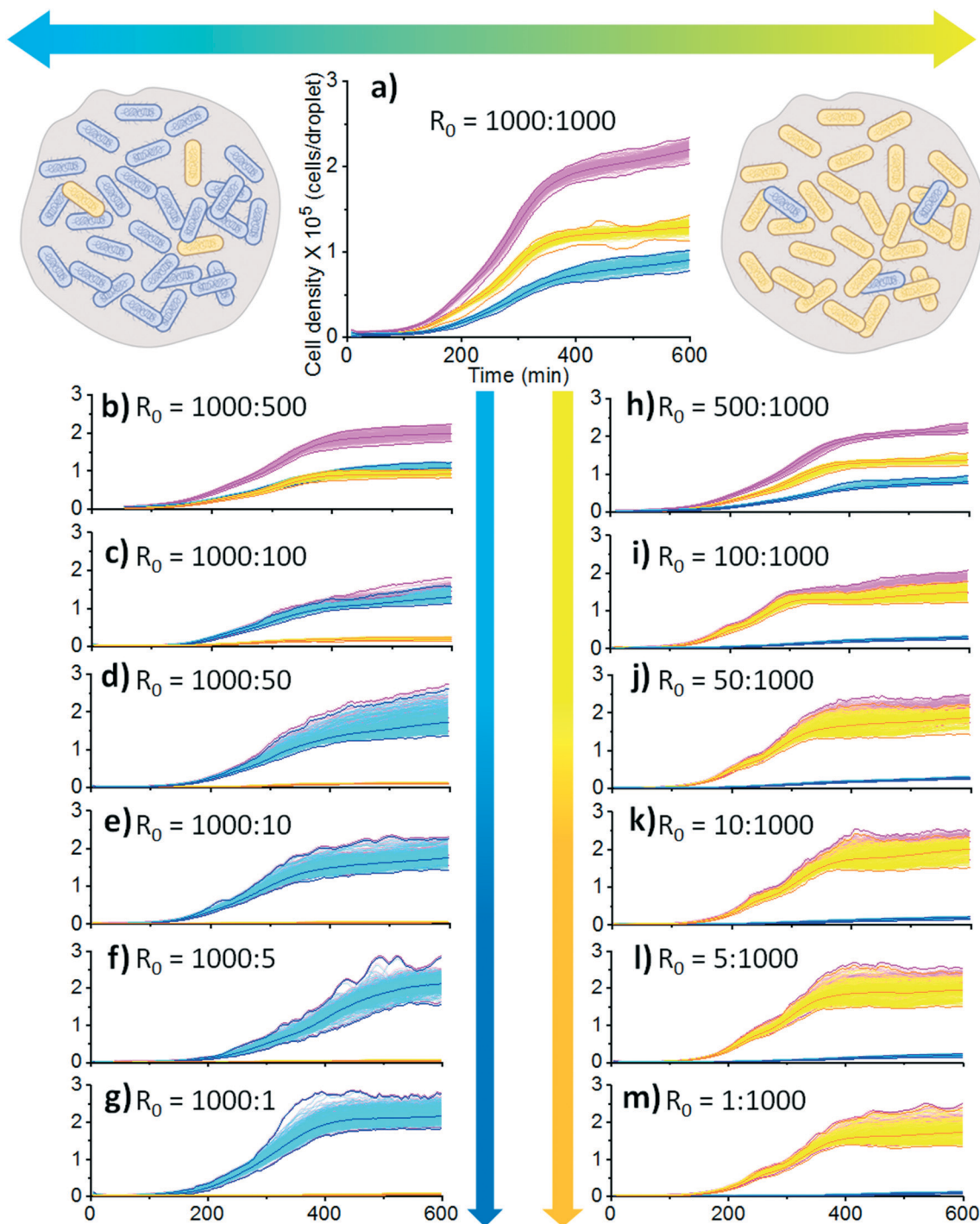


**Fig. 2** The combination (pink lines) of *E. coli* BFP (blue lines) and *E. coli* YFP (yellow lines) co-culture growth curves. The  $R_0$  of *E. coli* BFP: *E. coli* YFP are a) 1000:1000, b) 1000:500, c) 1000:100, d) 1000:50, e) 1000:10, f) 1000:5, g) 1000:1, h) 500:1000, i) 100:1000, j) 50:1000, k) 10:1000, l) 5:1000, m) 1:1000.

previous conclusion that the lower the relative initial frequency, the higher its relative yield.

Similar to final biomass, the doubling time of each strain also varies with the change of the  $R_0$ . Unlike in the monoculture case, both *E. coli* strains' doubling time changes in the co-culture case with different  $R_0$  (Fig. 3b and S15<sup>†</sup>). Relative to the monoculture, the addition of another bacterial

strain in a co-culture environment reduces both strains' growth rates in varying degrees. The magnitude of this effect depends on the  $R_0$ . Notably, the doubling time  $\tau$  of *E. coli* YFP is lower than that of *E. coli* BFP, even when  $R_0$  equals 10. However, once the inoculated cell number of the slower strain *E. coli* BFP is higher than those of YFP ( $R_0 > 1$ ), doubling time  $\tau_B$  does not change substantially, while  $\tau_Y$

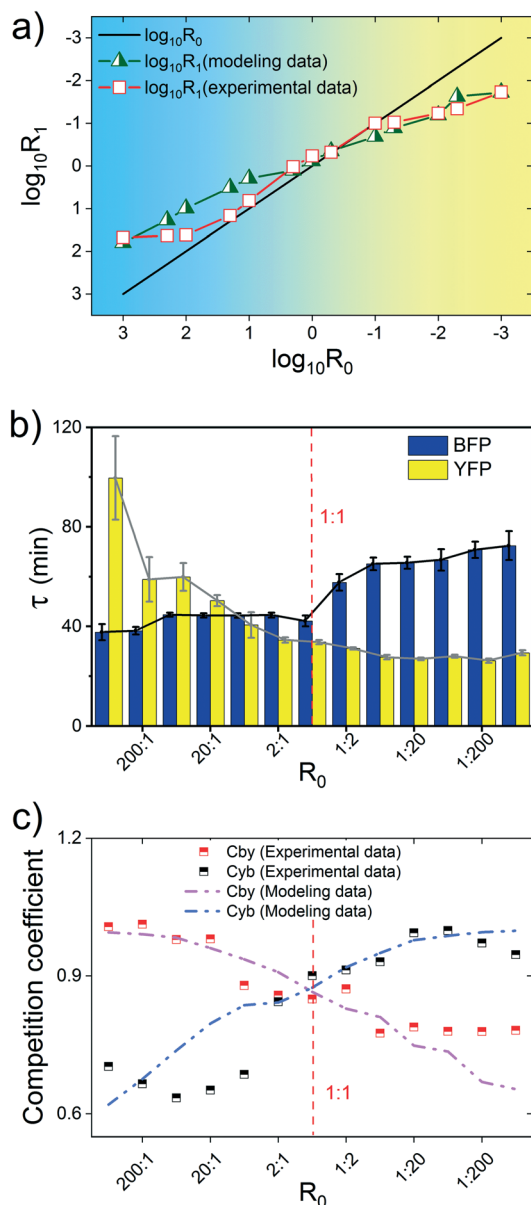


**Fig. 3** Comparison of biomass at the beginning of the stationary phase and doubling time between two strains of *E. coli* with different  $R_0$ . Comparison of a)  $R_1$  ( $R_1 = B_1/Y_1$ , the biomass ratio at the beginning of the stationary phase between *E. coli* BFP and *E. coli* YFP) and b) doubling time of each strain in co-culture as a function of  $R_0$ . c) Comparison of the competition coefficients calculated based on experimental data and modeling data.

increases superlinear (Fig. S13b†). In the opposite case, once *E. coli* YFP dominates ( $R_0 \ll 1$ ),  $\tau_Y$  stays unchanged at a certain value, while  $\tau_B$  reveals slow quadratic function growth (Fig. S13a†). It seems that the larger initial fraction bacterial strain becomes dominant with its fraction increasing.<sup>44</sup> Based on these results, we speculate that the larger initial cell density helps the bacteria get more access to the nutrients for their cell division efficiently. The adding of other strains does not influence its doubling time much. Conversely, the growth of the fewer fraction bacteria is affected more and more when its fraction decreased.

We further checked the doubling time by culturing bacteria in 96 wells plates and measuring in the plate reader (see details in Fig. S10†). Besides, we also compared the doubling time obtained from co-culture prediction results in Fig. S14.† All results reveal similar patterns as in the droplet analyzer. But all the doubling times in 96 wells are slower than in other culture and detect methods. We ascribed this phenomenon to limited mixing during culturing, which is unfavorable to bacterial growth.<sup>45</sup>

Finally, the competition coefficient ( $C_{by}$  and  $C_{yb}$ ) between two co-culture strains was calculated and compared from experimental data and modeling data (Fig. 3c). We found that as  $R_0$  decreased,  $C_{by}$  and  $C_{yb}$  show diametrically opposite and symmetrical trends. It indicates that the strain with a higher initial frequency suppresses the growth of the other strain, irrespective of the marker. Remarkably, this unequal effect strengthens with  $R_0$  change from 1 to extreme ratios of  $10^3$  or  $10^{-3}$ .

### Competition distribution map

To more intuitively display how the  $R_0$  affects the relationship between two *E. coli* strains, the doubling time of two strains from each droplet is presented in a two-dimensional (2D) distribution map in Fig. 4.<sup>28</sup> Lower doubling times mean faster growth rate, which leads to a competitive advantage. The 2D distribution map is divided into four regions by the average monoculture doubling time of each strain (blue dotted line and yellow dotted line). As a result of the competition for resources, one strain's growth can be affected by the other due to nutrients domination, toxic releasing, or even predation.<sup>9</sup> The four regions were named as Cooperation, Advantage\_Y, Advantage\_B, and Competition, based on the relative doubling times of both strains. If co-culture results in a shorter doubling time than monoculture for both strains, it is an indication that they are benefiting from each other's cooperation, hence this region is called 'Cooperation'. *Vice versa* situation we name 'Competition'.

Compared to the monoculture clouds (black dots, randomly paired of the monoculture doubling time of the two *E. coli* strains), the co-culture clouds (red dots, doubling time of the two *E. coli* strains from each droplet was paired) shifted to the direction of the competition region (see Fig. 4a). When  $R_0 < 1$  (yellow box in Fig. 4h-m), the co-culture clouds (red dots) shifted directly to the Advantage\_Y region. Moreover, as  $R_0$  deviates from 1, the co-culture clouds (red dots) further moved to the Advantage\_Y region. Differently, when  $R_0 > 1$  (Fig. 4b-g), the co-culture clouds (red dots) shifted to the competition region first, and then with  $R_0$  increased, they moved to the Advantage\_B region. The distribution of dots was also summarized and compared in Table S3 (ESI†). In both cases, there is a gradual trend that when the initial cell density fraction of one *E. coli* strain dominates and continuously rises, the co-culture clouds finally move to the Advantage region. The two different movement pathways also reveal differences in the

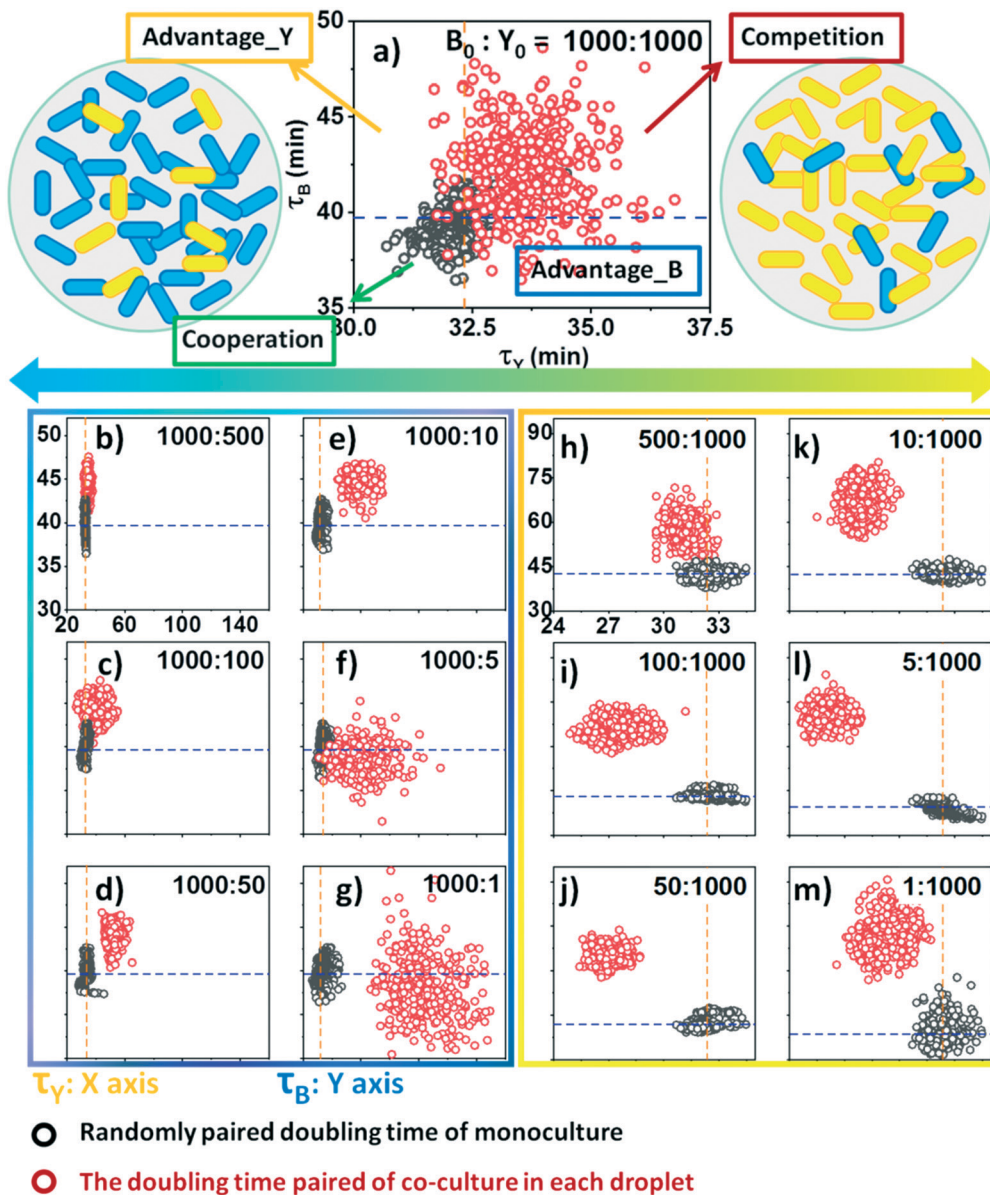


Fig. 4 Correlation between doubling time of the two strains of *E. coli*: monoculture (black dots, randomly paired), and co-culture in the droplet (red dots) with  $R_0$  of *E. coli* BFP: *E. coli* YFP. a) 1000 : 1000, b) 1000 : 500, c) 1000 : 100, d) 1000 : 50, e) 1000 : 10, f) 1000 : 5, g) 1000 : 1, h) 500 : 1000, i) 100 : 1000, j) 50 : 1000, k) 10 : 1000, l) 5 : 1000, and m) 1 : 1000. The blue dotted line and yellow dotted line separately represent the average doubling time of *E. coli* BFP and *E. coli* YFP in monoculture case.

competitiveness of the two bacterial strains in the co-culture environment, *i.e.*, the *E. coli* YFP is stronger than *E. coli* BFP. Furthermore, the co-culture clouds dispersion range becomes more expansive as the  $R_0$  change from 1 to  $10^{-3}$  (more frequent of YFP) or  $10^3$  (more frequent of BFP). In other words, the variance of doubling time increases with decreasing inoculum. One possibility is that due to competition for resources, stochastic cell death happens, which affects smaller subpopulations more than larger subpopulations – hence the lower growth rate for small inocula.<sup>46–48</sup> A trade-off between growth rate and biomass yield (a faster growth comes with a lower yield and *vice versa*) may explain the negative frequency-dependence of final

biomass in co-culture. Further investigation should corroborate or reject these hypotheses, for which the droplet system described here may be a valuable tool.

## Experimental

### Batch culture

All *E. coli* were cultured in M9 (Sigma-Aldrich) compound medium with  $8 \text{ mg mL}^{-1}$  glucose (Sigma-Aldrich),  $1 \text{ mg mL}^{-1}$   $\text{MgSO}_4 \cdot 7\text{H}_2\text{O}$  (Sigma-Aldrich), and  $0.5 \text{ mg mL}^{-1}$  casein hydrolysate (Sigma-Aldrich) and incubated at  $37^\circ\text{C}$ . All bacteria were cultured overnight by shaking at 170 rpm for approximately 24 hours in a 100 mL flask containing 50 mL

of M9 compound medium. The growth curves and calculated doubling time of both strains display in Fig. S4.† The faster growth rate in the batch culture method is likely due to higher dissolved oxygen levels in flasks relative to other methods, including droplets. The YFP and BFP strains were constructed by inserting the fluorescent expression cassette, cat-J23101-SYFP2 (GenBank accession number: KM018300) or cat-J23101-mTagBFP2 (GenBank accession number: KM018299), into galK of *E. coli* MG1655 using the  $\lambda$  red recombineering system as described in Datsenko *et al.*<sup>49</sup> The chloramphenicol (cat) marker was removed after chromosomal integration using FLP recombinase. Both fluorescent proteins are expressed from the constitutive promoter, J23101.<sup>50</sup>

### Millifluidic droplet reactor culture

Bacteria were taken from fresh *E. coli* liquid medium, which were first pre-grown in fresh media for 3 hours to reach the early exponential growth phase. Bacteria were then diluted by a fresh M9 compound medium (store at 4 °C) in a 1.5 mL tube. Next, they were refilled into a 5 mL syringe and further encapsulated into a droplet with a volume of 200 nL. A droplet sequence with approximately 450 droplets was transferred forward and backward in front of the detectors at 37 °C for 20 hours.

### Droplet generation

The droplets were generated by T-junction and cross-junction in the water-in-oil system. The HFE oil (hydrofluoroether oil, C<sub>9</sub>H<sub>5</sub>F<sub>15</sub>O, Novec 7500, Ionic Liquids Technologies) and 1% surface-active agent (2% PicoSurf 1™, Dolomite) work as the continuous phase. Mineral oil (Sigma-Aldrich) serves as a spacer to separate the dispersed phase bacterial droplet. The two phases were injected into the FEP tubing (fluorinated ethylene propylene with an outer diameter of 1.6 mm and an inner diameter of 0.5 mm) using syringes which pumped with the flow rate ratio of HFE oil:mineral oil:medium = 1:5:5 (mL h<sup>-1</sup>). The generated droplets with spacers and HFP oil are shown in Fig. S16a.† The droplet is approximated as a cylindrical in shape (Fig. S16b and c†). Consequently, the volume of the droplet can be calculated using following equation:

$$V = (\pi/4) \times D^2 \times L, \quad (1)$$

where  $V$  is the volume of the droplet;  $D$  is the diameter of the droplet;  $L$  is the length of the droplet. The final volume of the droplet is calculated to be approximately 200 nL.

Moreover, droplet sequences with one or two cells in each droplet were generated and measured in the millifluidic device. Cell numbers were counted based on their bacterial growth curves in each droplet. The distributions of both *E. coli* BFP and *E. coli* YFP in each droplet are similar to the theoretical values of the Poisson distribution, as shown in Fig. S17.†

Taking into account preparation time for generating and injecting the droplets, scanning time for each cycle as well as the growth rate of the microbes, the number of droplets for each droplet sequence was chosen to be 450–500 droplets to keep the optimal time between consecutive measurements for each cycle.

### Cell density calculation by biophotometer (OD<sub>600</sub>)

The cell density of *E. coli* was measured by Biophotometer (Eppendorf) and calculated with the following formula (M9 compound medium). Before measuring the cell density, the bacterial media was first diluted into the measuring range of  $0 \leq OD_{600} \leq 1$ . Then, the result is obtained by multiplying the dilution factor.

$$\text{Cell density} = 5.1 \times 10^8 \times OD_{600} (0 \leq OD_{600} \leq 1) \quad (2)$$

### Millifluidic droplet detectors-spectrometer

A fiber-coupled spectrometer (QE65000, Ocean Optics) was used with a wavelength range from 200 nm to 1100 nm. Due to the different refractive index numbers between the medium droplet and mineral oil, the two kinds of droplets show different intensities when pass by the detection area. The spectrometer signal vibration peaks tell the location of the droplet sequence.

### Millifluidic droplet detectors-PMT

The fluorescence signal emitted from *E. coli* was detected by a susceptible photomultiplier tube (PMT, H10722-20, Hamamatsu) with a spectral range from 230 nm to 920 nm. The BFP detection mode contains an LED light source (385 nm, Thorlabs) and a BFP filter set (390/18 nm excitation and 460/60 nm emission, Thorlabs). The YFP detection mode contains an LED light source (505 nm, Thorlabs) and a YFP filter set (497/16 nm excitation and 535/22 nm emission, Thorlabs).

According to the relationship between droplet number and cycle time (with a flow rate of 5 mL h<sup>-1</sup>) shown in Fig. S18,† it takes 418 s (450 droplets) for co-culture (209 s for monoculture) for a measurement. The obtained growth curves are point-by-point data and shown as continuous curves.

### Cell density calculation by droplets analyzer

The calibration curves of cell density (cells per droplet)-fluorescent intensity were obtained by detecting bacterial medium with different dilution under PMT (Fig. S2†), the PMT signal was collected and further calibrated with cell density measured by OD<sub>600</sub>. The calibration curves of the two strains are shown in the following formulas:

$$E. coli \text{ BFP cell density} = 2.9975 \times 10^5 \times FDA - 2.7742 \times 10^4 \quad (3)$$

$$E. coli \text{ YFP cell density} = 1.1995 \times 10^6 \times FDA - 7.4108 \times 10^4 \quad (4)$$

Also, we checked the possibility of a signal cross. The *E. coli* BFP solution was diluted to the same concentrations with M9 and the original *E. coli* YFP solution, respectively (Fig. S3a†). The *E. coli* BFP diluted with these two different solutions had the same intensity of the signal at the same dilution factors, indicating that the addition of *E. coli* YFP does not alter the *E. coli* BFP signal. Similarly, Fig. S3b† demonstrates *E. coli* BFP does not affect the detection of *E. coli* YFP. In Fig. S3c† and d, two bacterial strains' signal interference was examined using the extreme cell density ratio from 1:100 to 1:900. In both assays, only the larger strains showed the signal changes that matched the calibration curve. In comparison, the smaller strains maintained the baseline level, demonstrating that the two assays' signals of co-cultured strains did not interfere with each other.

### Calculation of the doubling time

According to the generation rate equation in the exponential phase, the steepest slope was taken to calculate the growth rate in all growth curves.<sup>51,52</sup>

$$\text{Growth rate} = (\log_2 N_b - \log_2 N_a) / (T_b - T_a) = [\log_2(N_b/N_a)] / (T_b - T_a) \quad (5)$$

$N$  Cell number (cells).

$C$  Cell concentration or cell density (cells per mL).

$T$  Time (min).

a The point a on log scale cell numbers–time growth curve.

b The point b on log scale cell numbers–time growth curve.

Since,

$$N = C \times V = \text{OD}_{600} \times 5.1 \times 10^8 \times V = (c \times \text{FDA} \pm d) \times V \quad (6)$$

So,

$$\text{Growth rate} = [\log_2(C_b/C_a)] \times (T_b - T_a)^{-1} \quad (7)$$

$$= [\log_2(\text{OD}_b/\text{OD}_a)] \times (T_b - T_a)^{-1} \quad (8)$$

$$= \{\log_2[(c \times \text{FDA}_b \pm d) / (c \times \text{FDA}_a \pm d)]\} \times (T_b - T_a)^{-1} \quad (9)$$

$V$  Droplet volume, 200 nL.

$C$  Cell concentration or cell density (cells per mL).

$\text{OD}$  The optical density of a sample measured at a wavelength of 600 nm (A).

$c$  The slope of calibration curves for FAD.

$d$  The intercept of calibration curves for FAD.

$T$  Time (min)

$$\text{Doubling time} = (\text{Growth rate})^{-1} \quad (10)$$

Here, the range of bacterial cell density used to calculate the doubling time is within FAD's calibration curve. Besides, the calibration curves were measured, starting from a cell density below the LOD.

### Cell counting and biomass ratios at the beginning of the stationary phase

All bacteria samples were centrifuged and diluted by Phosphate buffered saline (PBS, Sigma-Aldrich) twice before detecting in a microscopy (Axiovert 200 M, Carl Zeiss) and flow cytometry (Attune NxT, Thermo Fisher). The co-culture group with  $R_0 = 1$  was observed under the fluorescence microscopy with a magnification of 40×. No clumps of two strains were observed (Fig. S8†). The  $R_1$  is calculated to be 0.798.

The *E. coli* BFP and *E. coli* YFP with various  $R_0$  were co-cultured for 8 hours and followed by centrifugation and dilution with PBS. The samples were then measured by flow cytometry. VL1 (440/50 nm) mode and BL1 (530/30 nm) mode were chosen for BFP and YFP detection, respectively. One example of the cytometry result ( $R_0 = 10^{-3}$ ) is shown in Fig. S9†. The cell numbers and biomass statistics are shown in Table S1†. For the  $R_1$  results detected in a plate reader (M200 Pro, Tecan), *E. coli* BFP and *E. coli* YFP were first pregrown in fresh media for 3 hours to reach the early exponential growth phase and then diluted by a fresh M9 compound medium. The two bacterial strains were then transferred into a black 96 well plate with the  $R_0$  from  $10^3$  to  $10^{-3}$  and measured every hour.

### The verification of the relationship between the fluorescent signals and the cell number

All *E. coli* samples were first cultured in M9 compound media in flasks by shaking at 170 rpm. After incubated for 0, 9, 24, and 36 hours, 3 mL media was taken from each sample and centrifuged 5 min with 3370 rpm (D-78532 Tuttlingen, Hettich). The supernatant was collected and measured with a pH meter (pH 1100 L, VWR). Then, 0.5 mL of the sample was diluted and observed with a microscopy, followed by further diluted to 20–50 cells per mL for preparing the solid LB agar in a petri dish (85 mm in diameter). The 500 mL LB agar solid media with 20 g L<sup>-1</sup> LB Broth (Sigma-Aldrich) and 15 g L<sup>-1</sup> Agar-agar (Merck) was first autoclaved under 121 °C for 15 min, then cool down to 46 °C. In each petri dish, 1 mL diluted bacterial sample (obtained from bacterial media at the time point of 9 h, 24 h, and 36 h) and 15 mL LB agar were well mixed and kept in an incubator with 37 °C for 36 hours.

### Calculation of the competition coefficient

The competition coefficient was calculated with the ratio of the Malthusian parameters<sup>37</sup> of the co-culture and monoculture:

$$C_{by} (\text{effect of } E. coli \text{ YFP on } E. coli \text{ BFP}) = \frac{[\ln(N_{b, \text{co-culture}, t=12 \text{ h}}/N_{b, \text{co-culture}, t=0 \text{ h}})]}{[\ln(N_{b, \text{monoculture}, t=12 \text{ h}}/N_{b, \text{monoculture}, t=0 \text{ h}})]} \quad (11)$$

$$C_{yb} (\text{effect of } E. coli \text{ BFP on } E. coli \text{ YFP}) = \frac{[\ln(N_{y, \text{co-culture}, t=12 \text{ h}}/N_{y, \text{co-culture}, t=0 \text{ h}})]}{[\ln(N_{y, \text{monoculture}, t=12 \text{ h}}/N_{y, \text{monoculture}, t=0 \text{ h}})]} \quad (12)$$

$N_b$  Cell number of *E. coli* BFP in either monoculture or co-culture case after incubating few hours.

$N_y$  Cell number of *E. coli* YFP in either monoculture or co-culture case after incubating few hours.

If  $C_{by} = 1$ , means *E. coli* YFP does not affect *E. coli* BFP, and *E. coli* BFP grows similar in monoculture compared to co-culture;  $C_{by} < 1$ : *E. coli* BFP is negatively affected by *E. coli* YFP;  $C_{yb} > 1$ : *E. coli* BFP is positively affected by the presence of *E. coli* YFP.

## Conclusions

To conclude, we successfully developed a system to study with high throughput the complex process of the bacterial coexistence, analyzing the growth curves of monoculture and co-culture *E. coli* BFP and *E. coli* YFP, and explained the interaction and relationship between them. The droplet-based millifluidic reactor allows culture and monitor two microbial strains in liquid media for the long-term. This strategy also achieved several goals, such as getting samples without affecting bacterial growth and real-time detection, automatic monitoring co-culture, and observe up to 1000 droplets at one time. Focusing on analyzing the two coexisting strains, we demonstrate the *E. coli* YFP grows slightly faster than *E. coli* BFP in monoculture case and sustains the advantage in co-culture case when  $R_0 < 2$ . The 2D doubling time distribution map intuitively shows the growth status of two bacterial strains in each droplet. By combining the modeling results with the experimental data, we proved a trade-off between growth rate and relatively biomass yield, and it is influenced by competition.

Compared to traditional bacterial detection equipment (such as Biophotometer, fluorescent microscopy, plate reader, and flow cytometry), our millidroplet reactor has shown advantages in coexistence studies. This system has a perspective to miniaturize microbial coexistence assays, allowing a controlled single-cell inoculum size, jellifying of the droplets *via* a combination of microfluidics with solid agar to encapsulate bacteria, *etc.* We envision this platform to be successful in further practical applications of multispecies studies, including drug-resistance at the clinical research level.

## Conflicts of interest

There are no conflicts to declare.

## Acknowledgements

We would like to thank Dr. Andy Farr for providing *E. coli* BFP strain and *E. coli* YFP strain. We thank Dr. Bergoí Ibarlucea for his bacteria culture experience and help. We thank Mr. Tao Huang for assistance with microscopy. We thank Prof. Dr. Lukas Geyrhofer for his valuable comments along with the development of this work. We also thank the China Scholarship Council for their support.

## Notes and references

- 1 R. D. Holt, in *Spatial Heterogeneity, Indirect Interactions, and the Coexistence of Prey Species*, The University of Chicago, The American Naturalist, 1984, vol. 124, pp. 377–406.
- 2 P. Das, B. Ji, P. Kovatcheva-Datchary, F. Backhed and J. Nielsen, *PLoS One*, 2018, **13**, e0195161.
- 3 L. Keller and M. G. Surette, *Nat. Rev. Microbiol.*, 2006, **4**, 249–258.
- 4 M. E. Hibbing, C. Fuqua, M. R. Parsek and S. B. Peterson, *Nat. Rev. Microbiol.*, 2010, **8**, 15–25.
- 5 D. C. Savage, *Annu. Rev. Microbiol.*, 1977, **31**, 107–133.
- 6 T. D. Luckey, *Am. J. Clin. Nutr.*, 1970, **23**, 1430–1432.
- 7 E. M. M. Quigley, *Gastroenterol. Hepatol.*, 2013, **9**, 560–569.
- 8 R. A. Armstrong and R. Mcgrhee, *Theor. Popul. Biol.*, 1976, **9**, 317–328.
- 9 D. M. Cornforth and K. R. Foster, *Nat. Rev. Microbiol.*, 2013, **11**, 285–293.
- 10 Z. Danku, M. Perc and A. Szolnoki, *Sci. Rep.*, 2019, **9**, 262.
- 11 L. Geyrhofer and N. Brenner, *BMC Ecol.*, 2020, **20**, 1–23.
- 12 D. Tilman, F. Isbell and J. M. Cowles, *Annu. Rev. Ecol. Evol. Syst.*, 2014, **45**, 471–493.
- 13 B. Kerr, M. A. Riley, M. W. Feldman and B. J. M. Bohannan, *Nature*, 2002, **418**, 171–174.
- 14 H. Kaji, G. Camci-Unal, R. Langer and A. Khademhosseini, *Biochim. Biophys. Acta*, 2011, **1810**, 239–250.
- 15 J. Cairns, R. Jokela, J. Hultman, M. Tamminen, M. Virta and T. Hiltunen, *Front. Genet.*, 2018, **9**, 312.
- 16 L. Goers, P. Freemont and K. M. Polizzi, *J. R. Soc., Interface*, 2014, **11**, 20140065.
- 17 H. Ahern, *Microbiology: A Laboratory Experience*, Open SUNY Textbooks, State University of New York, Geneseo, 2018.
- 18 D. Lopez and R. Kolter, *FEMS Microbiol. Rev.*, 2010, **34**, 134–149.
- 19 D. R. Bogdanowicz and H. H. Lu, *Biotechnol. J.*, 2013, **8**, 395–396.
- 20 M. S. Thogersen, J. Melchiorson, C. Ingham and L. Gram, *Front. Microbiol.*, 2018, **9**, 1705.
- 21 H. Iwade, M. Yamada, N. Kimura, R. Hashimoto, Y. Yajima, R. Utoh and M. Seki, *Sens. Actuators, B*, 2019, **287**, 486–495.
- 22 P. Acai, A. Medved'ova, T. Mancuskova and L. Valik, *Food Sci. Technol. Int.*, 2019, **25**, 692–700.
- 23 K. Stephens, M. Pozo, C. Y. Tsao, P. Hauk and W. E. Bentley, *Nat. Commun.*, 2019, **10**, 4129.
- 24 J. A. Jones and X. Wang, *Curr. Opin. Biotechnol.*, 2018, **53**, 33–38.
- 25 G. J. Kremers, S. G. Gilbert, P. J. Cranfill, M. W. Davidson and D. W. Piston, *J. Cell Sci.*, 2011, **124**, 157–160.
- 26 C. M. Southward and M. G. Surette, *Mol. Microbiol.*, 2002, **45**, 1191–1196.
- 27 D. Kaushal, L. Ma, G. Zhang and M. P. Doyle, *PLoS One*, 2011, **6**, e18083.
- 28 X. Guo, K. P. T. Silva and J. Q. Boedicker, *Phys. Biol.*, 2019, **16**, 036001.
- 29 S. S. Terekhov, I. V. Smirnov, A. V. Stepanova, T. V. Bobik, Y. A. Mokrushina, N. A. Ponomarenko, A. A. Belogurov, Jr., M. P. Rubtsova, O. V. Kartseva, M. O. Gomzikova, A. A. Moskovtsev, A. S. Bukatin, M. V. Dubina, E. S. Kostryukova, V. V. Babenko, M. T. Vakhitova, A. I. Manolov, M. V.

- Malakhova, M. A. Kornienko, A. V. Tyakht, A. A. Vanyushkina, E. N. Ilina, P. Masson, A. G. Gabibov and S. Altman, *Proc. Natl. Acad. Sci. U. S. A.*, 2017, **114**, 2550–2555.
- 30 D. Cottinet, F. Condamine, N. Bremond, A. D. Griffiths, P. B. Rainey, J. A. de Visser, J. Baudry and J. Bibette, *PLoS One*, 2016, **11**, e0152395.
- 31 L. Baraban, F. Bertholle, M. L. M. Salverda, N. Bremond, P. Panizza, J. Baudry, J. A. G. M. de Visser and J. Bibette, *Lab Chip*, 2011, **11**, 4057–4062.
- 32 R. Illing, D. Pfitzner, D. Jungmann, L. Baraban and G. Cuniberti, *Biomicrofluidics*, 2016, **10**, 024115-1-10.
- 33 J. Baranyi and T. A. Roberts, *Int. J. Food Microbiol.*, 1994, **23**, 277–294.
- 34 K. Gopalsamy, *J. Austral. Math. Soc. Ser. B*, 2009, **24**, 160–170.
- 35 Y. Ram, E. Dellus-Gura, M. Bibid, K. Karkaree, U. Obolskia, M. W. Feldmanb, T. F. Coopere, J. Bermand and L. Hadanya, *Proc. Natl. Acad. Sci. U. S. A.*, 2020, **117**, 13848.
- 36 S. Gude, E. Pince, K. M. Taute, A. B. Seinen, T. S. Shimizu and S. J. Tans, *Nature*, 2020, **578**, 588–592.
- 37 J. Concepcion-Acevedo, H. N. Weiss, W. N. Chaudhry and B. R. Levin, *PLoS One*, 2015, **10**, e0126915.
- 38 L. Huang, *Food Control*, 2013, **32**, 283–288.
- 39 M. H. Zwietering, F. M. Rombouts and K. van 't Riet, *J. Appl. Bacteriol.*, 1992, **72**, 139–145.
- 40 J. N. Henderson, H. Ai, R. E. Campbell and S. James Remington, *Proc. Natl. Acad. Sci. U. S. A.*, 2007, **104**, 6672–6677.
- 41 G. Jach and J. Winter, in *Studies in Natural Products Chemistry*, ed. A. Rahman, Elsevier, Germany, 2006, ch. 3, vol. 33, pp. 3–67.
- 42 P. J. Cranfill, B. R. Sell, M. A. Baird, J. R. Allen, Z. Lavagnino, H. M. de Gruiter, G. J. Kremers, M. W. Davidson, A. Ustione and D. W. Piston, *Nat. Methods*, 2016, **13**, 557–562.
- 43 in *Chemical Imaging Analysis*, ed. B. C. Adams Freddy, Elsevier, 2015, ch. 9, vol. 69, pp. 339–384.
- 44 B. R. Levin, F. M. Stewart and L. Chao, *Am. Nat.*, 1977, **111**, 3–24.
- 45 M. A. Juergensmeyer, E. S. Nelson and E. A. Juergensmeyer, *Lett. Appl. Microbiol.*, 2007, **45**, 179–183.
- 46 B. von Bronk, S. A. Schaffer, A. Gotz and M. Opitz, *PLoS Biol.*, 2017, **15**, e2001457.
- 47 A. J. McKane and T. J. Newman, *Phys. Rev. E: Stat., Nonlinear, Soft Matter Phys.*, 2004, **70**, 041902.
- 48 H. K. Alexander and C. MacLean, *Proc. Natl. Acad. Sci. U. S. A.*, 2020, **117**, 19455–19464.
- 49 K. A. Datsenko and B. L. Wanner, *Proc. Natl. Acad. Sci. U. S. A.*, 2000, **97**, 6640–6645.
- 50 J. R. Kelly, A. J. Rubin, J. H. Davis, C. M. Ajo-Franklin, J. Cumbers, M. J. Czar, K. de Mora, A. L. Gliberman, D. D. Monie and D. Endy, *J. Med. Biol. Eng.*, 2009, **3**, 1–13.
- 51 B. G. Hall, H. Acar, A. Nandipati and M. Barlow, *Mol. Biol. Evol.*, 2013, **31**, 232–238.
- 52 E. O. Powell, *J. Gen. Microbiol.*, 1956, **15**, 492–511.